Hinging Mechanisms of Masonry Single-Nave Barrel Vaults Subjected to Lateral and Gravity Loads

Haris Alexakis[1] and Nicos Makris, M.ASCE[2]

Abstract: This paper investigates the limit states of a circular masonry arch supported on rectangular buttresses when subjected to lateral inertial loading in addition to gravity loading by employing the principle of stationary potential energy. Depending on the slenderness of the arch compared to the slenderness of the buttresses, the study identifies two lower failure mechanisms: (1) a four-hinge mechanism within the arch alone; and (2) hinging of the arch in three locations together with a hinge at the base of the downstream buttress. In this analysis, radial ruptures are assumed for the arch, while the buttresses may rupture either horizontally or develop an oblique elongation failure along which the compression-free portion of the buttress separates. It is concluded that the hinging mechanism that triggers an oblique elongation failure of the downstream buttress is the most critical and initiates at a lower value of the seismic coefficient than the value associated with the mechanism that involves a horizontal fracture at the buttress. Finally, it is shown that the discrete-element method (DEM) captures the results of the proposed variational method with remarkable accuracy. **DOI: 10.1061/(ASCE)ST.1943-541X.0001762.** *© 2017 American Society of Civil Engineers.*

Author keywords: Stone arches; Buttresses; Minimum uplift acceleration; Energy methods; Limit-state analysis; Earthquake engineering; Seismic effects.

Downloaded from ascelibrary.org by University of Central Florida on 02/18/17. Copyright ASCE. For personal use only; all rights reserved.

Introduction

The main challenge in earthquake engineering in seeking to avoid collapse of a structural system is the correct identification of the lower collapse mechanism by appropriately locating the formation of imminent hinges. Once the lower collapse mechanism has been identified, one can proceed with a demand assessment analysis to estimate the level of lateral loading that a given structure can sustain before converting to a hinging mechanism. Historic structures built out of masonry are structural systems that essentially do not sustain any tension and the identification of the lower hinging mechanism is even more critical.

The planar seismic stability analysis of a masonry structure that does not sustain tension can be analyzed in two steps. Step A is an equivalent static-equilibrium stability analysis and deals with the calculation of the minimum horizontal acceleration, $\ddot{u}_g^{\text{up}}$, that is needed to rupture the structure at a minimum number of locations, which are sufficient to convert the structure into a mechanism. Step A is a purely geometric problem that is independent of the size (scale) of the structure and depends only on its slenderness. Step B deals with the postrupturing dynamic response analysis of a hinged structure that undergoes some rocking motion and involves the solution of the nonlinear equation of motion (Oppenheim 1992) while addressing satisfactorily the impact that happens whenever the motion reverses (De Lorenzis et al. 2007). Step B is a purely dynamic problem that involves participation of the rotational inertia of the articulated portions of the hinged structure; therefore, the postdynamic stability of the hinged structure depends strongly on its size (Makris 2014a, b).

This work focuses on identifying the lower hinging mechanism of a single-nave barrel vault, which is a masonry arch supported on two vertical buttresses as schematically shown in Fig. 1. Accordingly, this work concentrates in addressing Step A for the structural system shown in Fig. 1, since it is most relevant to a wide range of historic structures known as single-nave barrel-vault churches built in various parts of Europe as early as a millennia ago. For instance, Fig. 2(a) shows an exterior and interior view of the eleventh-century Church of Cedofeita (Portuguese: *Igreja de Cedofeita*) in Portugal; Fig. 2(b) shows the Church of San Juan in Spain, which was constructed between the twelfth and thirteenth centuries, and Fig. 2(c) shows the fifteenth-century Church of Saint George of the World (Greek: *Ιερά Μονή Αγίου Γεωργίου των Κουμάνων*) in Cyprus. The configuration of an arch (or vault) supported on buttresses is also often encountered as a substructure of more-complex masonry structures, such as romanesque or gothic cathedrals and Byzantine churches, medieval palaces and castles, or other simpler vaulted masonry structures that have been constructed throughout the world since the conception of the masonry arch (Huerta 2006; Roca et al. 2010). The planar analysis presented in this work assumes a plane-strain condition; therefore, it neglects the end effects of the front and back walls. Accordingly, the rupturing values of the seismic coefficient, ε, computed in this work are the low limit.

The level of ground shaking that is needed to initiate rupturing as calculated in Step A does not challenge the ultimate stability of the structure; however, it addresses the issue of locating the imminent hinges and rupturing of the masonry—an issue that is of utmost interest to the preservation efforts of cultural heritage.

For the simplest masonry structure, which is the monolithic free-standing column with base b and height h, Step A reduces to a simple static moment equilibrium since the structure is a one-hinge mechanism with the location of the hinges known a priori—the

[1]Postdoctoral Researcher, Dept. of Civil, Environmental and Construction Engineering, Univ. of Central Florida, Orlando, FL 32816.

[2]Professor, Dept. of Civil, Environmental and Construction Engineering, Univ. of Central Florida, Orlando, FL 32816; Member, Office of Theoretical and Applied Mechanics, Academy of Athens, Athina 106 79, Greece (corresponding author). E-mail: nicos.makris@ucf.edu

Note. This manuscript was submitted on June 23, 2016; approved on November 29, 2016; published online on February 14, 2017. Discussion period open until July 14, 2017; separate discussions must be submitted for individual papers. This paper is part of the ***Journal of Structural Engineering***, © ASCE, ISSN 0733-9445.

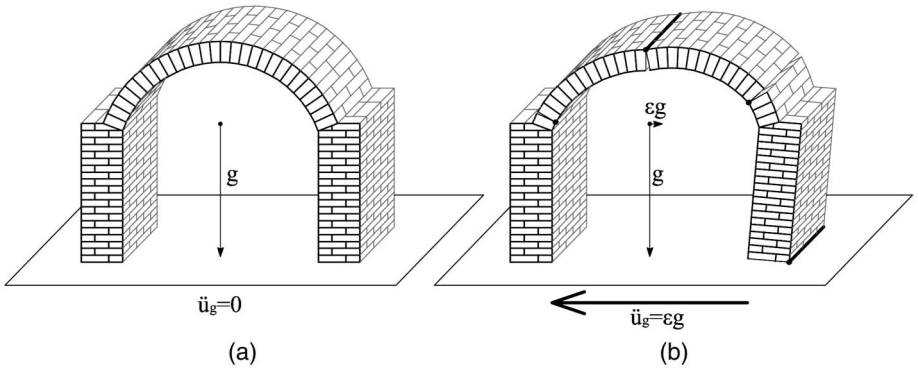


Fig. 1. (a) Single-nave barrel vault; (b) physically admissible hinge mechanism

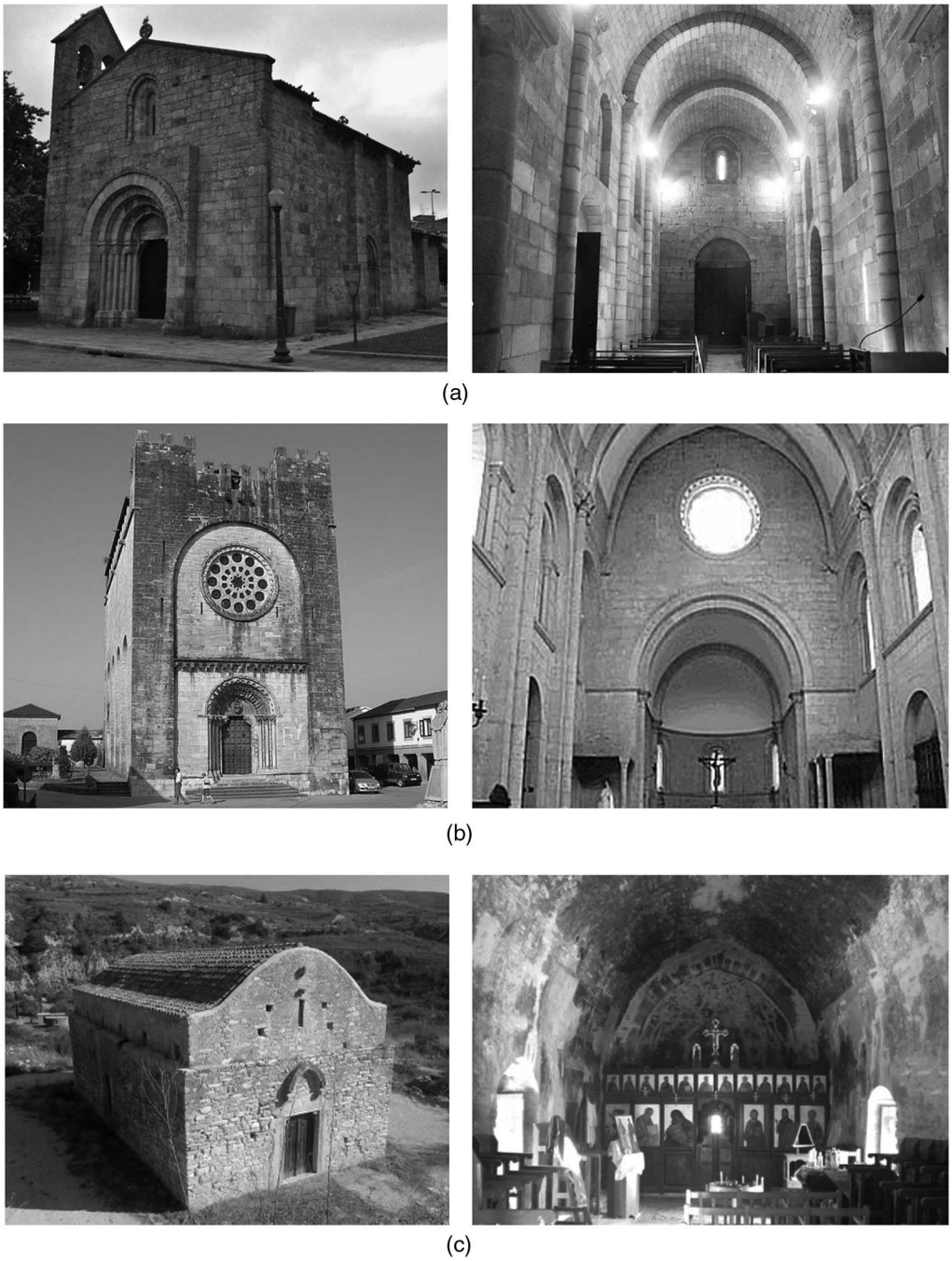


Fig. 2. Exterior and interior views of single-nave barrel-vault churches: (a) Church of Cedofeita, Porto, Portugal (eleventh century); (b) Church of San Juan, Portomarín, Spain (twelfth–thirteenth century); (c) Church of Saint George of the World, Mesana, Cyprus (fifteenth century)

Downloaded from ascelibrary.org by University of Central Florida on 02/18/17. Copyright ASCE. For personal use only; all rights reserved.

pivoting corner at its base. Accordingly, at the initiation of uplift (hinge formation) moment equilibrium gives that the uplift acceleration is merely $\ddot{u}_g^{up} = g(b/h) = g\tan\alpha$. In the case of a circular arched monolith with embrace angle β, midthickness radius R, and thickness t, that is about to become a four-hinge mechanism and initiate rocking motion, the calculation of the uplift acceleration $\ddot{u}_g^{up}/g = f(t/R, \beta)$ is less straightforward since the locations of the imminent hinges is not known a priori. Consequently, when studying the limit equilibrium of arches or single-nave barrel-vault structures subjected to lateral loads, one faces the challenge of computing the locations of the four hinges.

In his pioneering study on masonry arches under lateral loads Oppenheim (1992) considered a circular arch that consists of seven voussoirs having eight radial joints. Accordingly, the imminent hinges in Oppenheim's arch can only occur at the predefined locations of the eight physical joints. Clemente (1998) further elaborated on the dynamic response and stability analysis of masonry arches subjected to a horizontal ground acceleration. In his work, the hinge mechanism and the value of the ground acceleration needed to initiate rocking are found by employing an iterative procedure that assumes an initial mechanism which is iteratively adjusted by satisfying simultaneously (1) the principle of virtual powers, and (2) in the converged mechanism, the corresponding thrust line can just be located within the profile of the arch. Consequently, Clemente's (1998) iterative method mixes elements from energy methods and from a geometric formulation that involves the limiting thrust line. More recently, Alexakis and Makris (2014) presented a straightforward application of the principle of stationary potential energy to compute the value of the rupture/uplift acceleration of circular arches together with the locations of the four imminent hinges. Based on a rigorous variational formulation, the Alexakis and Makris (2014) study shows that the exact value of the rupture/uplift acceleration depends on the stereotomy exercised and settles the problem of the limit equilibrium analysis of masonry structures using energy methods without the need to involve the geometric concept of the thrust line (see also Makris and Alexakis 2013; Alexakis and Makris 2013, 2015). These theoretical efforts come to support recent trends for the seismic-performance assessment of historic structures by employing the limit equilibrium of substructure elements to develop retrofitting guidelines (Lagomarsino and Cattari 2015).

In this paper, the variational methodology advanced by Alexakis and Makris (2014) is employed to find the limit equilibrium configuration of the single-nave barrel vault shown in Fig. 1, given that the buttresses that support the arch may develop an oblique elongation failure (Heyman 1992; Ochsendorf 2002; Ochsendorf et al. 2004; Makris and Alexakis 2015).

Physically Admissible Hinging Mechanisms of a Single-Nave Barrel Vault

De Luca et al. (2004) presented a simplified iterative procedure for the seismic demand assessment of the structural system shown in Fig. 1. Their methodology combines linear finite-element (FE) and limit-state analysis with the use of the principle of virtual work applied in preselected failure mechanisms. De Luca et al. (2004) examined three types of hinging mechanisms: (1) the local mechanism where the mechanism is formed only by three portions of the arch (Mechanism I in Fig. 3); (2) semiglobal mechanism where the arch and one of the buttresses participate in the hinging mechanism (Mechanism II in Fig. 3); and (3) global mechanism where the entire structural system forms a hinging mechanism where both buttresses uplift (Mechanism III in Fig. 3). This paper examines these three kinematically admissible mechanisms together with two additional mechanisms, namely Mechanisms IV and V shown in Fig. 3, which are between the semiglobal and global mechanism by permitting one of the ruptures to happen horizontally inside the downstream (right) or upstream (left) buttress, respectively (in Fig. 3, it is assumed that the lateral inertial forces are applied from the left).

If an arch that may support its own weight is relatively slender and/or the buttresses relatively stocky, the four-hinge lateral mechanism develops only within the arch, as shown in Fig. 3 (Mechanism I), while the buttresses do not participate in the mechanism. This is precisely the problem of identifying the limit equilibrium state of a circular masonry arch under lateral inertial and gravity loads—a problem that has been studied by Clemente (1998) and more recently by Alexakis and Makris (2014), who presented a rigorous variational formulation in an effort to liberate the limit-state analysis from the need to identify the limiting thrust line. Accordingly, the exact locations of the imminent hinges and the level of horizontal ground acceleration εg that is needed to mobilize the hinging Mechanism I in Fig. 3 has been presented in detail in the paper by Alexakis and Makris (2014). It was first recognized by Clemente (1998) that if the arch is subjected to a lateral load (say from the left

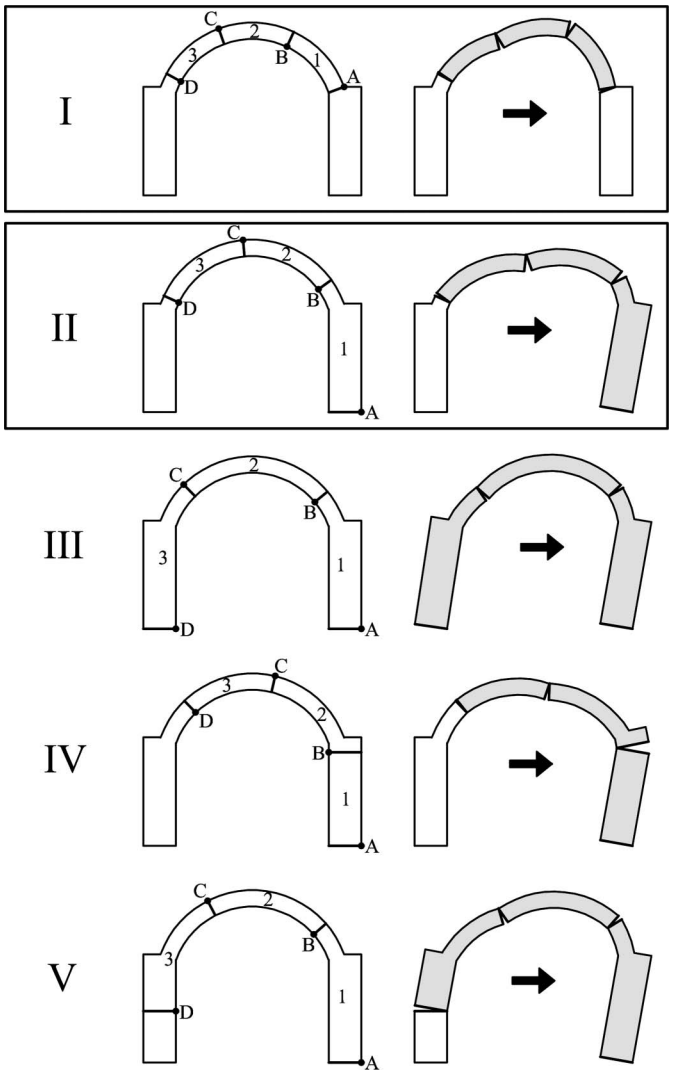


Fig. 3. Among the five physically admissible hinging mechanisms shown, only the top two are lower failure mechanisms for buttresses that are allowed to develop horizontal ruptures

Downloaded from ascelibrary.org by University of Central Florida on 02/18/17. Copyright ASCE. For personal use only; all rights reserved.

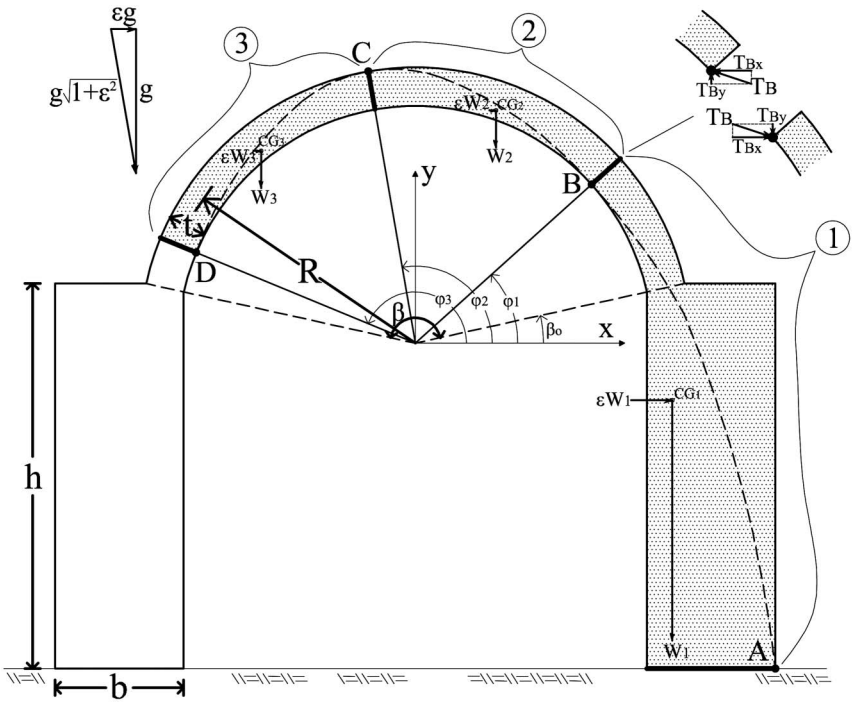


Fig. 4. Formation of a four-hinge semiglobal mechanism (Mechanism II in Fig. 3) in a circular arch supported on two rectangular buttresses when subjected to a horizontal ground acceleration $\ddot{u}_g = \varepsilon g$

to the right), the extreme right extrados hinge always happens at the right Springing A, while the extreme left intrados Hinge D may happen within the arch at a location above the left springing (one-springing mechanism), or at the left springing (two-springing mechanism). In that way, the location of Hinge A is known, and the analysis searches for the three unknown locations of Hinges B, C, and D, together with the level of the lateral load that initiates the mechanism.

If an arch capable of supporting its own weight is relatively thick and/or the buttresses relatively slender, the location of the extrados Hinge A shall be transferred to the bottom right corner of the downstream buttress, in an analogy to the arch mechanism, and the analysis searches again for the three unknown locations of Hinges B, C, and D, together with the level of the lateral load that initiates any of the Mechanisms II–V in Fig. 3.

The next section applies the principle of stationary potential energy, initially employed in Alexakis and Makris (2014) to calculate the exact location of the hinges and the level of the limit horizontal inertial loading, εg, for any given geometry of a single-nave barrel-vault structure that does not sustain tension.

Mechanism II: Semiglobal Mechanism that Initiates a Horizontal Rupture at the Base of the Buttress

With reference to Fig. 4, consider a circular arch with embrace angle, β, midthickness radius, R, and thickness, t, that is supported on two rectangular buttresses with height, h, and width, b. The structure is subjected to a constant horizontal ground acceleration εg (say from left to right). Prior to hinging, the structure translates as a rigid body; therefore, the lateral inertial loading will assume a profile proportional to the vertical distribution of the mass.

Moment equilibrium of Segment 2 (Segment BC) about Hinge C gives

$$-\varepsilon W_2\left[\left(R+\frac{t}{2}\right)\sin\phi_2 - y_2\right] + W_2\left[x_2 - \left(R+\frac{t}{2}\right)\cos\phi_2\right] + T_{Bx}\left[\left(R+\frac{t}{2}\right)\sin\phi_2 - \left(R-\frac{t}{2}\right)\sin\phi_1\right] - T_{By}\left[\left(R-\frac{t}{2}\right)\cos\phi_1 - \left(R+\frac{t}{2}\right)\cos\phi_2\right] = 0 \quad (1)$$

In Eq. (1), T_{Bx} and T_{By} = Cartesian components of the unknown thrust force T_B acting at Hinge B (Fig. 4); and W_2, x_2, and y_2 = weight and Cartesian coordinates of the center of gravity of Segment 2, which are functions of the unknown rupture locations φ_1 and φ_2

$$W_2 = tR(\phi_2 - \phi_1) \quad (2)$$

$$x_2 = R\frac{\sin\phi_2 - \sin\phi_1}{\phi_2 - \phi_1}\left(1 + \frac{1}{12}\frac{t^2}{R^2}\right) \quad (3)$$

$$y_2 = -R\frac{\cos\phi_2 - \cos\phi_1}{\phi_2 - \phi_1}\left(1 + \frac{1}{12}\frac{t^2}{R^2}\right) \quad (4)$$

Moment equilibrium of the combined Segment 2–3 (Segment BCD) about Hinge D gives

$$\varepsilon W_{2-3}\left[y_{2-3} - \left(R-\frac{t}{2}\right)\sin\phi_3\right] + W_{2-3}\left[x_{2-3} - \left(R-\frac{t}{2}\right)\cos\phi_3\right] - T_{Bx}\left[\left(R-\frac{t}{2}\right)\sin\phi_1 - \left(R-\frac{t}{2}\right)\sin\phi_3\right] - T_{By}\left[\left(R-\frac{t}{2}\right)\cos\phi_1 - \left(R-\frac{t}{2}\right)\cos\phi_3\right] = 0 \quad (5)$$

In Eq. (5), W_{2-3}, x_{2-3}, and y_{2-3} = weight and Cartesian coordinates of the center of gravity of the combined Segment 2–3,

Downloaded from ascelibrary.org by University of Central Florida on 02/18/17. Copyright ASCE. For personal use only; all rights reserved.

which are functions of the unknown rupture locations φ_1 and φ_3

$$W_{2-3} = tR(\phi_3 - \phi_1) \tag{6}$$

$$x_{2-3} = R\frac{\sin\phi_3 - \sin\phi_1}{\phi_3 - \phi_1}\left(1 + \frac{1}{12}\frac{t^2}{R^2}\right) \tag{7}$$

$$y_{2-3} = -R\frac{\cos\phi_3 - \cos\phi_1}{\phi_3 - \phi_1}\left(1 + \frac{1}{12}\frac{t^2}{R^2}\right) \tag{8}$$

Moment equilibrium of Segment 1 (Segment AB) about Hinge A gives

$$\begin{aligned}\varepsilon W_1\left[y_1 + h - \left(R + \frac{t}{2}\right)\sin\beta_o\right] - W_1\left[\left(R - \frac{t}{2}\right)\cos\beta_o + b - x_1\right]\\ + T_{Bx}\left[\left(R - \frac{t}{2}\right)\sin\phi_1 + h - \left(R + \frac{t}{2}\right)\sin\beta_o\right]\\ - T_{By}\left[\left(R - \frac{t}{2}\right)\cos\beta_o + b - \left(R - \frac{t}{2}\right)\cos\phi_1\right] = 0\end{aligned} \tag{9}$$

In Eq. (9), $\beta_o = (\pi - \beta)/2$ = angle that form the springings with the horizontal axis; and W_1, x_1, and y_1 = weight and Cartesian coordinates of the center of gravity of Segment 1, which are functions of the unknown rupture location ϕ_1. Segment 1 consists of three areas: the sum of the rectangular buttress area, A_b, and the arch segment area, A_a, subtracting the triangular area that is formed from their intersection, A_t. The weight and the Cartesian coordinates of the center of gravity of Segment 1 can then be given by

$$W_1 = W_b + W_a - W_t \tag{10}$$

$$x_1 = \frac{x_b W_b + x_a W_a - x_t W_t}{W_1} \tag{11}$$

$$y_1 = \frac{y_b W_b + y_a W_a - y_t W_t}{W_1} \tag{12}$$

where

$$W_b = bh \tag{13}$$

$$x_b = \left(R - \frac{t}{2}\right)\cos\beta_o + \frac{b}{2} \tag{14}$$

$$y_b = \left(R + \frac{t}{2}\right)\sin\beta_o - \frac{h}{2} \tag{15}$$

$$W_a = tR(\phi_1 - \beta_o) \tag{16}$$

$$x_\alpha = R\frac{\sin\phi_1 - \sin\beta_o}{\phi_1 - \beta_o}\left(1 + \frac{1}{12}\frac{t^2}{R^2}\right) \tag{17}$$

$$y_\alpha = -R\frac{\cos\phi_1 - \cos\beta_o}{\phi_1 - \beta_o}\left(1 + \frac{1}{12}\frac{t^2}{R^2}\right) \tag{18}$$

$$W_t = \frac{t^2}{2}\sin\beta_o\cos\beta_o \tag{19}$$

$$x_t = \left(R - \frac{t}{6}\right)\cos\beta_o \tag{20}$$

$$y_t = \left(R + \frac{t}{6}\right)\sin\beta_o \tag{21}$$

Substitution of Eqs. (1) and (5) into Eq. (9) eliminates the unknown force components T_{Bx} and T_{By} and yields a transcendental equation that involves (1) geometric parameters β, t/R, b/R, and h/R; (2) rupture locations φ_1, φ_2, and φ_3; and (3) seismic coefficient ε. In the event of a demand assessment analysis (finding the level of loading that a given structure can sustain), the geometry of the buttressed arch is given and the analysis searches for the seismic coefficient ε that initiates the hinge mechanism. The solution of the aforementioned transcendental equation can then be expressed in the form

$$\varepsilon = f(\phi_1, \phi_2, \phi_3) \tag{22}$$

The analysis proceeds with the application of the principle of stationary potential energy by adopting a new reference level shown in Fig. 5, and tilting the structure by an angle ω such that $\tan\omega = \varepsilon$. Given the equivalent static representation of the horizontal acceleration εg adopted in this paper, the resultant acceleration field $g\sqrt{1+\varepsilon^2}$ is also inclined at an angle ω in a way that the new gravitational field has been enhanced by the term $\sqrt{1+\varepsilon^2}$ (Gaß 1990; Ochsendorf 2002; DeJong 2009; Alexakis and Makris 2014). In the tilted configuration of Fig. 5, the potential energy expresses the entire energy of the system (the work of all forces) and is given by

$$\begin{aligned}V &= \sqrt{1+\varepsilon^2}W \cdot y_o \quad \text{or}\\ V(\phi_1, \phi_2, \phi_3) &= \sqrt{1 + f(\phi_1, \phi_2, \phi_3)^2}W \cdot y_o\end{aligned} \tag{23}$$

where W = weight of the leveled buttressed arch; and y_o = ordinate of the center of gravity relative to the new reference level of Fig. 5.

According to the principle of stationary potential energy, the geometrically admissible hinged mechanism is in an equilibrium state if and only if the total potential energy of the system is stationary ($\delta V = 0$). Since in this case, the potential energy $V(\varphi_1, \varphi_2, \text{and } \varphi_3)$ is a function of three variables φ_1, φ_2, and φ_3,

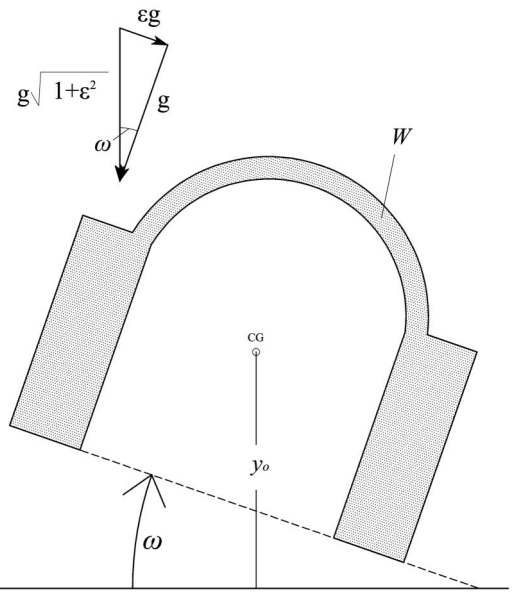


Fig. 5. Tilted buttressed arch by an angle $\omega = \tan^{-1}(\varepsilon)$ [new gravitational field has intensity $g\sqrt{(1+\varepsilon^2)}$]

Downloaded from ascelibrary.org by University of Central Florida on 02/18/17. Copyright ASCE. For personal use only; all rights reserved.

the potential energy is stationary when (Shames and Dym 1985, among others)

$$\frac{\partial V(\phi_1, \phi_2, \phi_3)}{\partial \phi_1} = 0 \tag{24}$$

$$\frac{\partial V(\phi_1, \phi_2, \phi_3)}{\partial \phi_2} = 0 \tag{25}$$

and

$$\frac{\partial V(\phi_1, \phi_2, \phi_3)}{\partial \phi_3} = 0 \tag{26}$$

Substitution of Eq. (23) to any of the Eqs. (24)–(26) ($j \in \{1,2,3\}$) gives

$$\frac{\partial V(\phi_1, \phi_2, \phi_3)}{\partial \phi_j} = \frac{\partial f(\phi_1, \phi_2, \phi_3)}{\partial \phi_j} W y_o \frac{f(\phi_1, \phi_2, \phi_3)}{\sqrt{1 + f(\phi_1, \phi_2, \phi_3)^2}} = 0, \quad j \in \{1,2,3\} \tag{27}$$

Given that the structure has a finite thickness and is capable of sustaining its own weight [$f(\varphi_1, \varphi_2, \varphi_3) = \varepsilon \neq 0$] and that y_o is also nonzero, Eq. (27) vanishes only when

$$\frac{\partial f(\phi_1, \phi_2, \phi_3)}{\partial \phi_j} = \frac{\partial \varepsilon}{\partial \phi_j} = 0, \qquad j \in \{1,2,3\} \tag{28}$$

Eq. (22) together with the three equations from the expression in Eq. (28) ($j = 1,2,3$) offer a 4×4 system that can be solved numerically and calculate the four unknowns ε, φ_1, φ_2, and φ_3 for a given geometry of the structural system (β, t/R, b/R, and h/R). In addition, the following boundary conditions must be satisfied for Mechanism II:

$$\beta_o \leq \phi_1 < \phi_2 < \phi_3 \leq \pi - \beta_o \tag{29}$$

If a solution is found with $\varphi_1 < \beta o$ and/or $\varphi_3 > \pi - \beta o$, which represent Mechanisms IV or V shown in Fig. 3, the two extreme rupture angles are set as $\varphi_1 = \beta o$ and/or $\varphi_3 = \pi - \beta o$ and the 4×4 system reduces to a 3×3 system since φ_1 or φ_3 is known, or to a 2×2 system since both φ_1 and φ_3 are known.

Fig. 6 plots the seismic coefficient ε as a function of the arch thickness t/R for two values of buttress height, $h/R = 1$ and 2, which correspond to Figs. 6(a and b), respectively, for three values of the buttress width $b/R = 0.25$, 0.5, and 0.75 and for four values of the embrace angle $\beta = 180$, 155, 125, and 90° with dark solid line, gray solid line, dark dashed line, and gray dashed line, respectively.

The lines with positive slope correspond to the arch mechanism (Mechanism I in Fig. 3; see also Alexakis and Makris 2014), which is mobilized for relatively thin arches (low t/R). Clearly, in this mechanism, the dominant parameter is the embrace angle of the arch. Smaller embrace angles considerably increase the seismic resistance of the arch. For the mobilization of Mechanism I, the geometry of the buttress is immaterial; therefore, the same lines appear in Figs. 6(a and b).

If the arch is relatively thick, Mechanism II (Fig. 3) is mobilized first, which corresponds to the slightly horizontal branches. Clearly, in this mechanism, there is a small dependence of the arch geometry (β, t/R), while the dominant parameters are the dimensions of the buttress. For example, a slight increase of the buttress width might result in a significant increase of the seismic resistance. Tall slender buttresses that support a masonry arch, commonly found in historic structures (e.g., the nave of cathedrals), are more likely to rupture, even with relatively low peak ground acceleration.

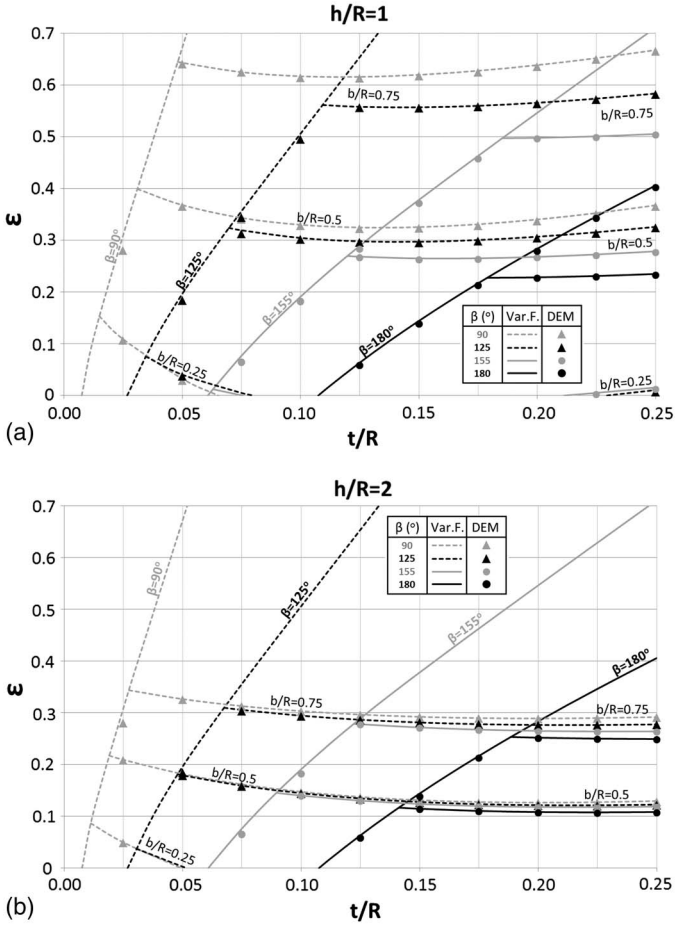


Fig. 6. Seismic coefficient ε for different geometries of the single-nave barrel vault with buttresses that are allowed to develop horizontal ruptures; lines = results from the variational formulation; isolated symbols = DEM results

This behavior is reminiscent to the behavior of a rocking frame, which consists of two free-standing columns (buttresses) capped with a rigid beam (epistyle). The seismic response of the rocking frame was recently studied in depth by Makris and Vassiliou (2013, 2014) and it was shown that the uplift acceleration is $\ddot{u}_g^{\text{up}}$, where b and h are the width and height of the vertical elements. When observing the results offered in Fig. 6, every family of lines that correspond to a given b/R is for a slenderness value of the buttress $b/h = (b/R)(R/h)$. Accordingly, Figs. 6(a and b) both indicate that the single-nave barrel vault always hinges at a lower value of the seismic coefficient that is capable of initiating uplift of the rocking frame, that is $\varepsilon = b/h$.

Tables 1 and 2 present indicative values of the seismic coefficient ε and rupture locations φ_1, φ_2, and φ_3, for

- Two values of the buttress height: $h/R = 1$ and 2, respectively;
- Three values of the arch thickness: $t/R = 0.05$, 0.15, and 0.25;
- One value of the buttress width: $b/R = 0.5$; and
- Four values of the embrace angle: $\beta = 180$, 155, 125, and 90°.

Values in italics correspond to Mechanism I (arch mechanism), while the rest correspond to Mechanism II. The empty rows for $t/R = 0.05$ and larger embracing angles are because the structure is not capable of sustaining its own weight. Values in bold correspond to the case where angles φ_1 or φ_3 indicate rupture exactly at the right or left springing of the arch.

Downloaded from ascelibrary.org by University of Central Florida on 02/18/17. Copyright ASCE. For personal use only; all rights reserved.

Table 1. Values of the Seismic Coefficient ε and Rupture Locations φ_1, φ_2, and φ_3, for Different Arch Configurations of a Single-Nave Barrel Vault with Buttresses Allowed to Develop Horizontal Ruptures and with Normalized Width $b/R = 0.5$ and Height $h/R = 1$

Single-nave barrel vault					Rocking frame
t/R	ε	φ_1 (degrees)	φ_2 (degrees)	φ_3 (degrees)	$\varepsilon = \frac{b}{h} = \frac{b}{R}\frac{R}{h}$
		$\beta = 180°$			—
0.05		—			—
0.15	*0.14433*	*40.439*	*98.212*	*155.987*	0.5
0.25	0.23483	41.035	103.215	165.396	0.5
		$\beta = 155°$			—
0.05		—			—
0.15	0.26489	47.062	104.836	162.610	0.5
0.25	0.27863	43.389	105.569	**167.5**	0.5
		$\beta = 125°$			—
0.05	*0.19642*	*54.314*	*101.113*	*147.911*	0.5
0.15	0.29717	48.332	105.615	**152.5**	0.5
0.25	0.32590	45.117	106.339	**152.5**	0.5
		$\beta = 90°$			—
0.05	0.36812	60.993	105.565	**135**	0.5
0.15	0.32546	47.241	101.862	**135**	0.5
0.25	0.36761	44.806	102.977	**135**	0.5

Note: Values in italics correspond to Mechanism I (arch mechanism); values in bold correspond to the case where angles φ_1 or φ_3 indicate rupture exactly at the right or left springing of the arch.

Table 2. Values of the Seismic Coefficient ε and Rupture Locations φ_1, φ_2, and φ_3 for Different Arch Configurations of a Single-Nave Barrel Vault with Buttresses Allowed to Develop Horizontal Ruptures and with Normalized Width $b/R = 0.5$ and Height $h/R = 2$

Single-nave barrel vault					Rocking frame
t/R	ε	φ_1 (degrees)	φ_2 (degrees)	φ_3 (degrees)	$\varepsilon = \frac{b}{h} = \frac{b}{R}\frac{R}{h}$
		$\beta = 180°$			—
0.05		—			—
0.15	0.11470	38.769	96.543	154.317	0.25
0.25	0.10842	34.008	96.188	158.368	0.25
		$\beta = 155°$			—
0.05		—			—
0.15	0.12391	39.290	97.064	154.837	0.25
0.25	0.11891	34.601	96.781	158.961	0.25
		$\beta = 125°$			—
0.05	0.17923	53.362	100.161	146.960	0.25
0.15	0.12779	39.488	97.239	**152.5**	0.25
0.25	0.12277	34.711	96.754	**152.5**	0.25
		$\beta = 90°$			—
0.05	0.18181	52.793	98.891	**135**	0.25
0.15	0.13121	**45**	95.002	**135**	0.25
0.25	0.12968	**45**	94.765	**135**	0.25

Note: Values in italics correspond to Mechanism I (arch mechanism); values in bold correspond to the case where angles φ_1 or φ_3 indicate rupture exactly at the right or left springing of the arch.

General Description of the Procedure and Its Application to Mechanisms III, IV, and V

The variational formulation methodology employed to identify Mechanism II (semiglobal mechanism) consists of five general steps that can be followed to compute any of the four-hinge mechanisms shown in Fig. 3:

- Step 1: Select three single or combined segments of the structural system and take three independent moment equilibrium equations about the hinges. All three equations must contain the unknown components of the same thrust force (applied at the same hinge location), while every unknown rupture position must be contained at least once in one of the equations;
- Step 2: Use any two of the three moment equilibrium equations and find the expressions of the two unknown components of the thrust force, by solving the 2×2 system;
- Step 3: Substitute the expressions of the force components into the third moment equilibrium equation. The new equation contains all three unknown rupture locations and all the geometrical parameters, together with the lateral load coefficient, ε;
- Step 4: Find the expression of ε and apply the principle of stationary potential energy that leads to three additional equations—that is, the partial derivative of ε about any of the three rupture locations of the mechanism must be zero; and
- Step 5: The equation of Step 3 together with the three equations of Step 4 can be used as a 4×4 system in order to find the three unknown rupture locations and the limit lateral force coefficient for a structural system with a given geometry.

The proposed variational formulation methodology was also applied to calculate the seismic coefficient, ε and the locations of the hinges associated with Mechanisms III, IV, and V shown in Fig. 3 and it was concluded that a higher seismic coefficient, ε, than the one identified with Mechanism II is needed to initiate hinging. Accordingly, when Mechanism I (arch mechanism) is not mobilized, Mechanism II is always the lower hinging mechanism for any geometry of the single-nave barrel vault; therefore, Mechanisms III, IV, and V do not materialize.

Mechanism II: Semiglobal Mechanism that Initiates an Oblique Elongation Rupture along the Buttress

A masonry buttress is not a monolithic column since it consists of individual stones placed roughly in horizontal courses and laid with or without mortar between the stones. In the event that the buttress is built out of large masonry blocks, the rupture may happen along the horizontal direction and mobilize Mechanism II shown in Fig. 3. In the event that the buttress is built out of smaller stones and the mortar has decayed with time, the buttress is incapable of sustaining any tension and eventually develops an elongation failure along the compression-free region (Heyman 1992; Ochsendorf 2002; Ochsendorf et al. 2004; Makris and Alexakis 2015).

Assuming a triangular stress distribution along the horizontal layers of the buttress and with reference to Fig. 7, the compression-free area originates at distance z from the head of the buttress, where the base of the triangular stress distribution is equal to the width of the buttress, b. Accordingly, Point M is the intersection point of the base of the triangular stress distribution and the trust line, located at distance $b/3$ from the external side of the buttress.

The most-critical fracture passes through the bottom corner of the buttress, as shown in Fig. 7 (Heyman 1992; Ochsendorf 2002; Ochsendorf et al. 2004; Makris and Alexakis 2015). Past studies (Ochsendorf et al. 2004; Makris and Alexakis 2015) have shown that under gravity loads alone, the buttresses shown in Fig. 7 will fail due to an inclined thrust from the arch at their top by developing an elongation failure that follows a straight line. If only inertial lateral loading is acting on a buttress that stands alone (no thrust force at its top), the exact shape of the fracture line is a slightly curved line (given by an error function), which however can be approximated with a straight line (Heyman 1992; Makris and Alexakis 2015). Herein, the combined event where the buttress supports

Downloaded from ascelibrary.org by University of Central Florida on 02/18/17. Copyright ASCE. For personal use only; all rights reserved.

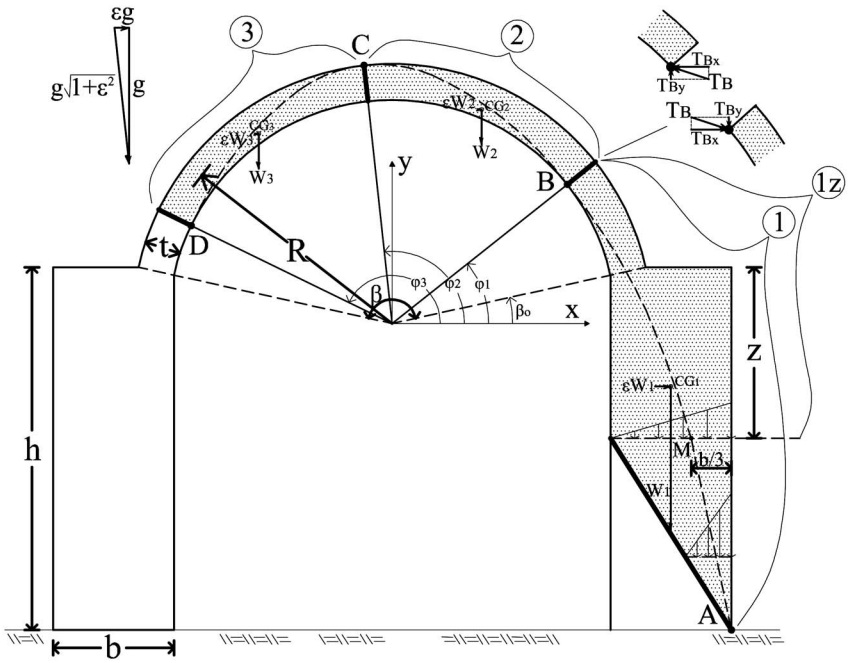


Fig. 7. Formation of a four-hinge mechanism for the case where the buttresses are allowed to develop an oblique elongation failure

the arch atop together with its own weight and the entire structure is subjected to lateral inertial loading is examined. Under this combined loading based on the discussion offered earlier, it is assumed that the fracture line is a straight line.

Ochsendorf (2002) recognizes that the height of the compression-free area depends on this combined action, although his analysis proceeds by considering only the horizontal thrust of the arch in the calculation for the height of the fracture. The variational formulation methodology presented in this paper permits the calculation of the critical distance, z, for the simultaneous action of gravity and lateral inertial loads; therefore accounting for all the forces acting at the structure. The distance z can be calculated by taking moment equilibrium of Segment $1z$ about Point M (Fig. 7), which gives

$$\begin{aligned}&\varepsilon W_{1z}\left[y_{1z}+z-\left(R+\frac{t}{2}\right)\sin\beta_o\right]\\&-W_{1z}\left[\left(R-\frac{t}{2}\right)\cos\beta_o+\frac{2b}{3}-x_{1z}\right]\\&+T_{Bx}\left[\left(R-\frac{t}{2}\right)\sin\phi_1+z-\left(R+\frac{t}{2}\right)\sin\beta_o\right]\\&-T_{By}\left[\left(R-\frac{t}{2}\right)\cos\beta_o+\frac{2b}{3}-\left(R-\frac{t}{2}\right)\cos\phi_1\right]=0\end{aligned}\tag{30}$$

In Eq. (30), W_{1z}, x_{1z}, and y_{1z} = weight and Cartesian coordinates of the center of gravity of Segment $1z$ (Fig. 7), given by

$$W_{1z}=W_z+W_a-W_t\tag{31}$$

$$x_{1z}=\frac{x_zW_z+x_aW_a-x_tW_t}{W_{1z}}\tag{32}$$

$$y_{1z}=\frac{y_zW_z+y_aW_a-y_tW_t}{W_{1z}}\tag{33}$$

where

$$W_z=bz\tag{34}$$

$$x_z=\left(R-\frac{t}{2}\right)\cos\beta_o+\frac{b}{2}\tag{35}$$

$$y_z=\left(R+\frac{t}{2}\right)\sin\beta_o-\frac{z}{2}\tag{36}$$

and W_a, x_a, y_a, W_t, x_t, and y_t are given by Eqs. (16–21).

The rest of the process is identical to what has been presented earlier. The only difference is that in the moment equilibrium equation of Segment 1 [Eq. (9)] W_1, x_1, and y_1 have changed due to the presence of the compression-free area, which does not participate in the mechanism. In this case

$$W_1=W_{1z}+W_f\tag{37}$$

$$x_1=\frac{x_{1z}W_{1z}+x_fW_f}{W_1}\tag{38}$$

$$y_1=\frac{y_{1z}W_{1z}+y_fW_f}{W_1}\tag{39}$$

where W_f, x_f, and y_f = weight and Cartesian coordinates of the center of gravity of the triangular shaded area that forms the fracture between Points A and M shown in Fig. 7; and are given by

$$W_f=\frac{1}{2}b(h-z)\tag{40}$$

$$x_f=\left(R-\frac{t}{2}\right)\cos\beta_o+\frac{2b}{3}\tag{41}$$

$$y_f=\left(R+\frac{t}{2}\right)\sin\beta_o-\frac{h+2z}{3}\tag{42}$$

Downloaded from ascelibrary.org by University of Central Florida on 02/18/17. Copyright ASCE. For personal use only; all rights reserved.

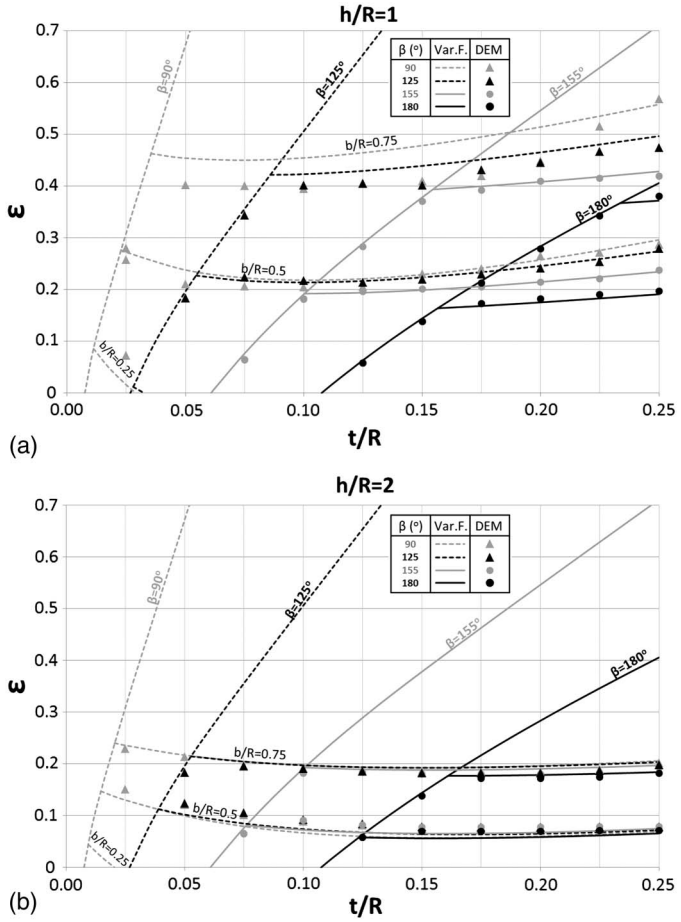


Fig. 8. Seismic coefficient ε for different geometries of the single-nave barrel vault with buttresses that are allowed to develop an oblique elongation failure; lines = results from the variational formulation; isolated symbols = DEM results

Fig. 8 and Tables 3 and 4 offer the corresponding critical values presented in Fig. 6 and Tables 1 and 2, respectively, for the case where the buttress develops an elongation failure. The lines with the positive slope in Fig. 8 that represent the arch mechanism (Mechanism I in Fig. 3) remain the same; meanwhile, the slightly horizontal lines of Mechanism II reveal a significant reduction of the seismic capacity due to the oblique elongation failure. Tables 3 and 4 include two additional columns: (1) dimensionless distance z/h, and (2) percentage of the reduction of the seismic coefficient ε compared with the case of a horizontal rupture at the base of the buttress, where the entire height of the buttress counterbalances the lateral forces. For the range of the values used in this parametric analysis depicted in Fig. 8 ($t/R = 0$–0.25, $\beta = 90 - 180°$, $h/R = 1$–2, and $b/R = 0.25$–0.75) the initiation of rupture z/h ranges from $0.38 \le z/h \le 0.62$ while the reduction of the seismic coefficient compared to the case of a horizontal rupture varies from approximately 10–60% or occasionally even higher.

Validation of the Discrete-Element Method

Over the last two decades, an increasing number of engineers have been using the discrete-element method (DEM) for the analysis of masonry structures and monuments in an effort to capture the discontinuous nature of masonry (Cundall 1971; Pagnoni 1994; Lemos 1995, 2007; Papantonopoulos et al. 2002, among others). In this paper, the results presented in Figs. 6 and 8 are compared with the results obtained with DEM analysis, where the commercially available software *UDEC* (Universal Distinct Element Code) has been used. Recently, Alexakis and Makris (2016) presented a validation of DEM for the limit stability analysis of masonry arches where DEM reproduces the analytical results with remarkable accuracy.

In order for the DEM results to be comparable with those of limit equilibrium analysis, the stone blocks must be considered

Table 3. Values of the Seismic Coefficient ε and Rupture Locations φ_1, φ_2, and φ_3 for Different Arch Configurations of a Single-Nave Barrel Vault with Buttresses Allowed to Develop an Oblique Elongation Failure and with Normalized Width $b/R = 0.5$ and Height $h/R = 1$

t/R	ε	φ_1 (degrees)	φ_2 (degrees)	φ_3 (degrees)	z/h	Reduction (%)
			$\beta = 180°$			
0.05			—			
0.15	*0.14433*	*40.439*	*98.212*	*155.987*	—	—
0.25	0.19092	38.629	100.809	162.989	0.47846	18.7
			$\beta = 155°$			
0.05			—			
0.15	0.19898	43.480	101.254	159.028	0.49706	24.9
0.25	0.23433	41.008	103.188	165.369	0.55114	15.9
			$\beta = 125°$			
0.05	*0.19642*	*54.314*	*101.113*	*147.911*	—	—
0.15	0.22357	44.632	102.188	**152.5**	0.54050	24.8
0.25	0.27400	42.601	104.092	**152.5**	0.60182	15.9
			$\beta = 90°$			
0.05	0.23786	55.448	101.152	**135**	0.45338	35.4
0.15	0.22891	**45**	98.574	**135**	0.54506	29.7
0.25	0.29605	**45**	100.613	**135**	0.61606	19.5

Note: Values in italics correspond to Mechanism I (arch mechanism); values in bold correspond to the case where angles φ_1 or φ_3 indicate rupture exactly at the right or left springing of the arch.

Table 4. Values of the Seismic Coefficient ε and Rupture Locations φ_1, φ_2, and φ_3 for Different Arch Configurations of a Single-Nave Barrel Vault with Buttresses Allowed to Develop an Oblique Elongation Failure and with Normalized Width $b/R = 0.5$ and Height $h/R = 2$

t/R	ε	φ_1 (degrees)	φ_2 (degrees)	φ_3 (degrees)	z/h	Reduction (%)
			$\beta = 180°$			
0.05			—			
0.15	0.05639	35.454	93.228	151.002	0.40003	50.8
0.25	0.06584	31.586	93.767	155.947	0.46089	39.3
			$\beta = 155°$			
0.05			—			
0.15	0.06555	35.976	93.750	151.524	0.44038	47.1
0.25	0.07503	32.110	94.291	156.471	0.50052	36.9
			$\beta = 125°$			
0.05	0.10222	49.038	95.836	142.636	0.39731	43.0
0.15	0.06461	35.923	93.697	151.471	0.45037	49.4
0.25	0.07262	31.938	94.073	**152.5**	0.51112	40.8
			$\beta = 90°$			
0.05	0.09967	48.626	95.156	**135**	0.38930	45.2
0.15	0.05723	**45**	92.198	**135**	0.42694	56.4
0.25	0.07008	**45**	92.586	**135**	0.49474	46.0

Note: Values in italics correspond to Mechanism I (arch mechanism); values in bold correspond to the case where angles φ_1 or φ_3 indicate rupture exactly at the right or left springing of the arch.

Downloaded from ascelibrary.org by University of Central Florida on 02/18/17. Copyright ASCE. For personal use only; all rights reserved.

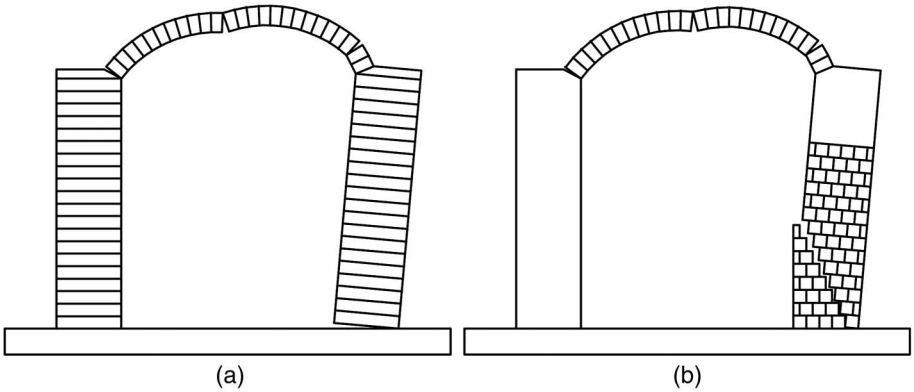


Fig. 9. Models used in DEM analysis with (a) buttresses that are allowed to develop horizontal ruptures only; (b) buttresses that are allowed to develop an elongation failure

as rigid, while the angle of friction between the joints, φ, must be large enough (e.g., $\varphi \geq 80°$) to prevent sliding. In addition, the effect of the mortar has been neglected and the tensile strength, cohesion, and dilatancy angle shall be zero.

The method adopts an elastic behavior that leads to the need to define the normal-to-the-contact surface, K_n (normal stiffness), and tangential-to-contact-surface, K_s (shear stiffness), equivalent linear-elastic constants. The variation of these values has a marginal effect on the assessment of the limit state that is the minimum seismic coefficient ε and the imminent hinging mechanism. By using values between 10^7 and 10^9 Pa/m the algorithm converges fast and with reliable results. In this analysis $K_n = K_s = 10^8$ Pa/m.

The material density does not appear in the equations of limit analysis, which is governed by geometry. The DEM confirms this behavior since very small or very large values of density have been tested without affecting the results of the limit equilibrium analysis. In this analysis, the density was chosen to be 2,000 kg/m^3. Similarly, it was confirmed that the results of the analysis remain invariant to scale; $R = 1$ m was chosen.

Fig. 9 presents the discretized models that were used: Fig. 9(a) for Case A, where the buttresses are allowed to rupture horizontally at any height, and Fig. 9(b) for Case B, where the buttresses are allowed to develop an oblique elongation failure. All voussoirs have size = 5°, which means that the arches with embrace angle $\beta = 180$, 155, 125, and 90° have 36, 31, 25, and 18 voussoirs, respectively. The same discretization was satisfactorily used by Alexakis and Makris (2014) to reproduce the collapse mechanisms of circular arches under lateral and gravity loads. The gravity load and horizontal inertia load corresponding to each block are applied as static loads at the center of gravity of each block.

For Case A, all buttresses are divided into 20 identical rectangular blocks and one trapezoidal block at the head, as shown in Fig. 9(a). The circular and triangular points in Fig. 6 represent the results obtained with DEM for all the range of t/R values with a step of 0.025. The circular black dots correspond to the solid black line for $\beta = 180°$. The circular gray dots correspond to the solid gray line for $\beta = 155°$. The triangular black points correspond to the dashed black line for $\beta = 125°$. The triangular gray points correspond to the dashed gray line for $\beta = 90°$. The numerical solution of DEM is in excellent agreement with the theoretical solution from the variational formulation. It is confirmed that the buttress uplifts without developing any intermediate horizontal ruptures and the location of the four hinges match those predicted from the theoretical solution.

For Case B, a finer discretization was chosen for the buttress in order to capture the diagonal failure, as shown in Fig. 9(b). In principle, the finer the discretization, the better the elongation failure that can be reproduced. However, for a large number of blocks, the algorithm does not converge. For this reason, given that the theoretical solution predicted that the distance $z/h > 0.38$, the upper 30% of the right buttress was not discretized together with the left buttress, where diagonal fracture is not expected. The size of the square blocks of the right buttress was chosen as $0.1R$. The dots in Fig. 8 represent the results obtained with DEM. Given that there is a slight deviation between the exact area of the discretized buttress that uplifts compared with the theoretical one, the results are still in good agreement.

Conclusions

By employing the principle of stationary potential energy, this paper identifies the lower hinging mechanism of a single-nave barrel vault, i.e., a circular masonry arch supported on rectangular buttresses when subjected to lateral inertial loading in addition to gravity loading.

Depending on the relative slenderness of the arch to the slenderness of the buttress, the paper identifies two lower failure mechanisms: (1) hinging of the arch alone—that is, a mechanism where the buttresses do not participate as if the arch was supported on the ground; and (2) hinging of the arch together with a hinge at the base of the downstream buttress.

In this analysis, radial ruptures are assumed for the arch; meanwhile, the buttress may either rupture horizontally or develop an oblique elongation failure along which the compression-free portion of the buttress separates. In the event that the buttresses are built out of large masonry blocks and the rupture happens along a horizontal direction (entire buttress uplifts), the single-nave barrel vault ruptures with a seismic coefficient ε that is always smaller than the slenderness of the buttresses = b/h. As the embracing angle of the arch diminishes, the single-nave barrel vault hinges at a higher value of the seismic coefficient, which, however, remains lower than the hinging seismic coefficient of the rocking frame, which is $\varepsilon = b/h$.

The paper concludes that the hinging mechanism that triggers an oblique elongation failure of the downstream buttress is the most critical and initiates at a much lower value of the seismic coefficient, ε, than the mechanism that involves a horizontal fracture along the buttress. Values of the seismic coefficient, ε, that mobilize the lower hinging mechanisms have been presented in ready-to-use graphs and tables for various configurations of the single-nave barrel vault. Finally, the paper shows that DEM

Downloaded from ascelibrary.org by University of Central Florida on 02/18/17. Copyright ASCE. For personal use only; all rights reserved.

captures the results of the proposed variational method with remarkable accuracy.

References

Alexakis, H., and Makris, N. (2013). "Minimum thickness of elliptical masonry arches." *Acta Mech.*, 224(12), 2977–2991.

Alexakis, H., and Makris, N. (2014). "Limit equilibrium analysis and the minimum thickness of circular masonry arches to withstand lateral inertial loading." *Arch. Appl. Mech.*, 84(5), 757–772.

Alexakis, H., and Makris, N. (2015). "Limit equilibrium analysis of masonry arches." *Arch. Appl. Mech.*, 85(9), 1363–1381.

Alexakis, H., and Makris, N. (2016). "Validation of the discrete element method for the limit stability analysis of masonry arches." *Computational modeling of masonry structures using the discrete element method*, V. Sarhosis, K. Bagi, J. V. Lemos, and G. Milani, eds., IGI Global, Hershey, PA, 292–325.

Clemente, P. (1998). "Introduction to dynamics of stone arches." *Earthquake. Eng. Struct. Dyn.*, 27(5), 513–522.

Cundall, P. A. (1971). "A computer model for simulating progressive large-scale movements in blocky rock system." *Proc., Symp. of the Int. Society for Rock Mechanics*, Nancy, France.

DeJong, M. (2009). "Seismic assessment strategies for masonry structures." Ph.D. thesis, Dept. of Architecture, Massachusetts Institute of Technology, Boston.

De Lorenzis, L., DeJong, M., and Ochsendorf, J. (2007). "Failure of masonry arches under impulse base motion." *Earthquake. Eng. Struct. Dyn.*, 36(14), 2119–2136.

De Luca, A., Giordano, A., and Mele, E. (2004). "A simplified procedure for assessing the seismic capacity of masonry arches." *Eng. Struct.*, 26(13), 1915–1929.

Gaß, S. (1990). "IL 25: Experiments." Univ. of Lightweight Structures, Stuttgart, Germany.

Heyman, J. (1992). "Leaning towers." *Meccanica*, 27(3), 153–159.

Huerta, S. (2006). "Galileo was wrong: The geometrical design of masonry arches." *Nexus Network. J.*, 8(2), 25–52.

Lagomarsino, S., and Cattari, S. (2015). "PERPETUATE guidelines for seismic performance-based assessment of cultural heritage masonry structures." *Bull. Earthquake Eng.*, 13(1), 13–47.

Lemos, J. V. (1995). "Assessment of the ultimate load of a masonry arch using discrete elements." *Computer methods in structural masonry*, J. Middleton and G. N. Pande, eds., Books and Journals International, Swansea, U.K., 294–302.

Lemos, J. V. (2007). "Discrete element modelling of masonry structures." *Int. J. Archit. Heritage*, 1(2), 190–213.

Makris, N. (2014a). "A half-century of rocking isolation." *Earthquakes Struct.*, 7(6), 1187–1221.

Makris, N. (2014b). "The role of the rotational inertia on the seismic resistance of free-standing rocking columns and articulated frames." *Bull. Seism. Soc. Am.*, 104(5), 2226–2239.

Makris, N., and Alexakis, H. (2013). "The effect of stereotomy on the shape of the thrust-line and the minimum thickness of semicircular masonry arches." *Arch. Appl. Mech.*, 83(10), 1511–1533.

Makris, N., and Alexakis, H. (2015). "Limit equilibrium analysis of masonry buttresses and towers under lateral and gravity loads." *Arch. Appl. Mech.*, 85(12), 1915–1940.

Makris, N., and Vassiliou, M. F. (2013). "Planar rocking response and stability analysis of an array of free-standing columns capped with a freely supported rigid beam." *Earthquake. Eng. Struct. Dyn.*, 42(3), 431–449.

Makris, N., and Vassiliou, M. F. (2014). "Are some top-heavy structures more stable?" *J. Struct. Eng.*, 10.1061/(ASCE)ST.1943-541X.0000933, 06014001.

Ochsendorf, J. (2002). "Collapse of masonry structures." Ph.D. thesis, Dept. of Engineering, Univ. of Cambridge, Cambridge, U.K.

Ochsendorf, J. A., Hernando, J. I., and Huerta, S. (2004). "Collapse of masonry buttresses." *J. Archit. Eng.*, 10.1061/(ASCE)1076-0431(2004)10:3(88), 88–97.

Oppenheim, I. J. (1992). "The masonry arch as a four-link mechanism under base motion." *Earthquake Eng. Struct. Dyn.*, 21(11), 1005–1017.

Pagnoni, T. (1994). "Seismic analysis of masonry and block structures with the discrete element method." *Proc., 10th European Conf. on Earthquake Engineering*, A.A. Balkema, Rotterdam, Netherlands, 1669–1674.

Papantonopoulos, C., Psycharis, I. N., Papastamatiou, D. Y., Lemos, J. V., and Mouzakis, H. P. (2002). "Numerical prediction of the earthquake response of classical columns using the distinct element method." *Earthquake. Eng. Struct. Dyn.*, 31(9), 1699–1717.

Roca, P., Cervera, M., Gariup, G., and Pelà, L. (2010). "Structural analysis of masonry historical constructions. Classical and advanced approaches." *Arch. Comput. Methods. Eng.*, 17(3), 299–325.

Shames, I. H., and Dym, C. L. (1985). *Energy and finite elements methods in structural mechanics*, Hemisphere Publishing, New York.

UDEC version 4.0 [Computer software]. Itasca Consulting Group, Minneapolis.

Downloaded from ascelibrary.org by University of Central Florida on 02/18/17. Copyright ASCE. For personal use only; all rights reserved.